Nonlinear Model Predictive Control for the Polymorphic Transformation of L-Glutamic Acid Crystals

Martin Wijaya Hermanto and Min-Sen Chiu
Dept. of Chemical and Biomolecular Engineering, National University of Singapore, Singapore 117576

Richard D. Braatz
Dept. of Chemical and Biomolecular Engineering, University of Illinois at Urbana-Champaign, IL 61801

Polymorphism, a phenomenon where a substance can have more than one crystal forms, has recently become a major interest to the food, speciality chemical, and pharmaceutical industries. The different physical properties for polymorphs such as solubility, morphology, and dissolution rate may jeopardize operability or product quality, resulting in significant effort in controlling crystallization processes to ensure consistent production of the desired polymorph. Here, a nonlinear model predictive control (NMPC) strategy is developed for the polymorphic transformation of L-glutamic acid from the metastable α-form to the stable β-form crystals. The robustness of the proposed NMPC strategy to parameter perturbations is compared with temperature control (T-control), concentration control (C-control), and quadratic matrix control with successive linearization (SL-QDMC). Simulation studies show that T-control is the least robust, whereas C-control performs very robustly but long batch times may be required. SL-QDMC performs rather poorly even when there is no plant-model mismatch due to the high process nonlinearity, rendering successive linearization inaccurate. The NMPC strategy shows good overall robustness for two different control objectives, which were both within 7% of their optimal values, while satisfying all constraints on manipulated and state variables within the specified batch time. © 2009 American Institute of Chemical Engineers AIChE J, 55: 2631–2645, 2009
Keywords: pharmaceutical crystallization, polymorphism, nonlinear model predictive control, extended predictive self-adaptive control, unscented Kalman filter

Introduction

Polymorphism is a frequently encountered phenomenon for pharmaceutical compounds,[1] in which a substance can have more than one crystal forms, each with distinct properties. Because of the variation in physical properties such as crystal shape, solubility, hardness, color, melting point, and chemical reactivity, polymorphism is an important concern in the food, specialty chemical, and pharmaceutical industries, where products are specified not only by chemical composition but also by their performance. The unexpected appearance of a second polymorphic form of an active pharmaceutical ingredient used for the treatment of HIV, with substantially different dissolution and absorption characteristics, highlights the importance of polymorphism in the pharmaceutical industry.[2] In addition, the U.S. Food and Drug Administration (FDA) has tightened regulations for new drug applications to ensure that the drugs contain only the

desired polymorph. Controlling polymorphism to ensure consistent production of the desired polymorph is important, especially in the drug manufacturing industry where safety is paramount.

Up to now, the most widely adopted control strategy for crystallization process is T-control that determines a temperature profile by optimizing an objective function based on an offline nominal model.[3–7]* Although T-control is simple to implement, it has become well-known that it can be very sensitive to variations in the kinetic parameters.[8,9] This motivated the development of the robust T-control strategy which explicitly includes the impact of uncertainties in the objective while determining the optimal temperaturetime trajectory to be followed during batch operation.[10–12] With advances in sensor technologies, another control strategy developed to provide improved robustness to model uncertainty is C-control, which follows an optimal or nearly optimal concentration-temperature trajectory.[9,13–16] Despite the high impact of model predictive control (MPC)[17–23] in academic research and industrial practice, its application to solution crystallization processes has been rather limited.[24–29] One contribution considered the effects of uncertainties on the closed-loop performance of nonlinear model predictive control (NMPC) applied to crystallization processes.[27] As in many other papers, the method of moments was utilized to simplify the population balance equations which are partial differential equations (PDEs) to a set of ordinary differential equations (ODEs) in terms of the moments. The NMPC optimization problem was solved using nonlinear programming and the states were estimated using an extended Kalman filter (EKF).

To the authors' knowledge, there are no published results on the implementation of NMPC to a polymorphic crystallization, which is more challenging for a number of reasons. First, the phase equilibria and crystallization kinetics are more complicated. Second, the method of moments heavily used in past control algorithms for crystallization processes does not apply during a polymorphic transformation, so that the full PDEs need to be solved. As a consequence, the computation time required increases considerably, which prohibits the straightforward application of nonlinear programming. In this article a more practical NMPC strategy based on extended predictive self-adaptive control (EPSAC)[17,30–33] is developed for the polymorphic transformation of L-glutamic acid from the metastable α-form to the stable β-form. The polymorphic transformation process generally involves the dissolution of the metastable α-form crystals and the nucleation and growth of the stable β-form crystals. To implement the proposed NMPC strategy, an unscented Kalman filter (UKF)[34–38] is utilized to estimate the unmeasurable states. The performance and robustness of the proposed design is compared with T-control, C-control, and a standard NMPC algorithm in a numerical study.

This article is organized as follows. The next section summarizes the NMPC strategy based on EPSAC and UKF. Then the process model for polymorphic crystallization of L-glutamic acid is described, and the performance and robustness of the the proposed NMPC algorithm is compared to established control strategies. This is followed by conclu-

sions and an appendix that contains details on the NMPC control and estimation algorithms.

EPSAC-UKF NMPC Strategy

The optimal control problem to be solved online at every sampling instance in the NMPC algorithm is

$$\min_{u_k} J(x_k, u_k) \tag{1}$$

subject to

$$x_k = f(x_{k-1}, u_{k-1}) + w_k, \tag{2}$$

$$d_k = d_{k-1} + \xi_k, \tag{3}$$

$$y_k = g(x_k, u_k) + d_k + u_k, \tag{4}$$

$$h(x_k, u_k) \leq 0, \tag{5}$$

where J is the objective function; x_k, u_k, y_k, and d_k are the vectors of n_x system states, n_u inputs, n_y measured variables, and n_y unmeasured disturbances at the kth sampling instance; and w_k, ξ_k, and v_k are the vector of noises on the system states, unmeasured disturbances, and the measured variables. The system dynamics are described by the vector function f, the measurement equations by the vector function g, and the linear and nonlinear constraints for the system are described by the vector function h.

The key idea of EPSAC is to approximate nonlinear process variables by iterative linearization around future trajectories so that they converge to the same nonlinear optimal solution.[32] For this purpose, the future sequence of the input variables u_{k+i} is considered as the sum of a predetermined future control scenario $u_{b,k+i}$ and the optimizing future control actions δu_{k+i} (see Figure 1):

$$u_{k+i} = u_{b,k+i} + \delta u_{k+i}, \quad i = 0, 1, \ldots, N_u - 1, \tag{6}$$

where N_u is the control horizon and

$$\Delta u_{l,k} = \delta u_k,$$
$$\delta u_{k+m} = \sum_{j=0}^{m} \Delta u_{l,k+j},$$

Then the future trajectory of any process variables of interest (z_{k+i}) can be considered as being the cumulative result of two effects:

$$z_{k+i} = z_{b,k+i} + z_{l,k+i}, \tag{7}$$

where $z_{b,k+i}$ is calculated using the nonlinear model and predetermined sequence $u_{b,k+i}$. On the other hand, $z_{l,k+i}$ is obtained by an impulse response model with inputs $\{\delta u_k, \ldots, \delta u_{k+i-1}\}$. A similar decomposition into the sum of two parts is applied to the nonlinear constraints (5), to arrive at a quadratic program (QP). The soft-constraints approach[39] was used to provide numerical convergence of the QP optimizer. Details on the formulation and implementation of EPSAC are in the Appendix.

---

*To simpify the presentation, this text focuses on cooling crystallization; similar concepts apply to other methods of supersaturation generation such as antisolvent addition.
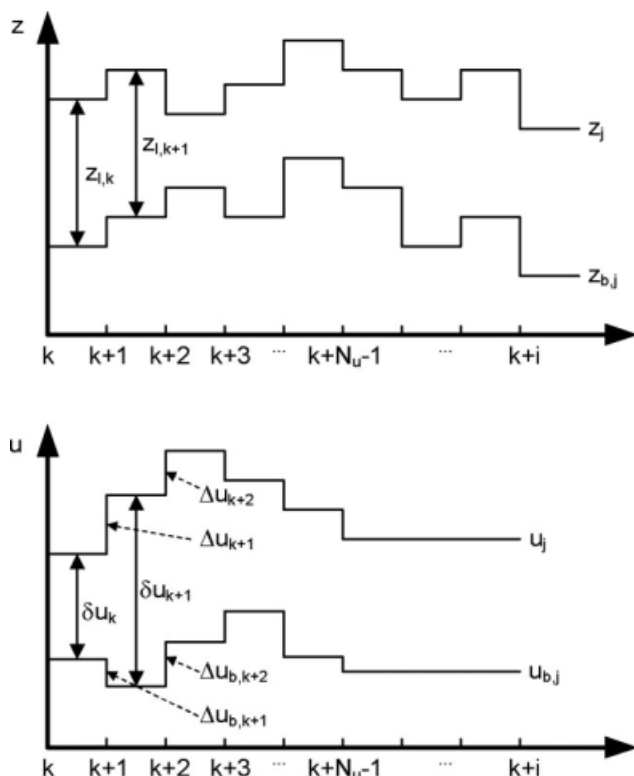
Figure 1. The variables decomposition in EPSAC.

In practice, not all states can be measured and those unmeasured states need to be estimated from available measurements. The most widely known state estimator for nonlinear systems is the extended Kalman filter (EKF). Although the EKF maintains the computationally efficient recursive update form of Kalman filter (KF), it has limitations. First, EKF relies on the linearization of the nonlinear system dynamics. The state estimates can be poor when the system is highly nonlinear. At worst, it may cause the state estimates to diverge. Secondly, linearization can be applied only if the Jacobian matrix exists. This means that EKF may not be applied to discontinuous systems. Finally, computing the Jacobian matrix can be poorly numerically conditioned for some processes.

Julier et al.[38] proposed an approach for filtering nonlinear systems to address the aforementioned problems by using what is now known as the unscented transformation (UT).[34–37] The UT works by constructing a set of points, referred as a sigma point, which are deterministically chosen to have the same known statistics (e.g., means and covariance) as a given state estimate. Then, a specified nonlinear transformation is applied to each sigma point, and the unscented estimate is obtained by computing the statistics of the transformed set. The incorporation of UT into the KF framework is called the unscented Kalman filter (UKF).[38] The appendix describes the implementation of UKF based on the spherical simplex unscented transformation.[35]

Description of the polymorphic crystallization process

This section summarizes the polymorphic crystallization model for metastable α-form and stable β-form crystals of L-Glutamic acid, which is similar to several models recently published in the literature.[40–42] The mass balances on the crystals are population balance equations:

$$\frac{\partial f_{\text{seed},i}}{\partial t} + \frac{\partial (G_i f_{\text{seed},i})}{\partial L} = 0, \tag{8}$$

$$\frac{\partial f_{\text{nucl},i}}{\partial t} + \frac{\partial (G_i f_{\text{nucl},i})}{\partial L} = B_i \delta(L - L_0), \tag{9}$$

where $f_{\text{seed},i}$ and $f_{\text{nucl},i}$ are the crystal size distributions of the i-form crystals (i.e., α- or β-form) obtained from seed crystals and nucleated crystals [#/m^4], B_i and G_i are the nucleation [#/m^{3}s] and growth rate [m/s] of the i-form crystals, L and L_0 are the characteristic size of crystals [m] and nuclei [m], and $\delta(\cdot)$ is the Dirac delta function.

The above equations are augmented by the solute mass balance:

$$\frac{dC}{dt} = -\frac{3 \times 10^3}{\rho_{\text{solv}}} (\rho_\alpha k_{v\alpha} G_\alpha \mu_{\alpha,2} + \rho_\beta k_{v\beta} G_\beta \mu_{\beta,2}), \tag{10}$$

where the nth moment of the i-form crystals #[m^{n-3}] is defined by

$$\mu_{i,n} = \int_0^\infty L^n (f_{\text{nucl},i} + f_{\text{seed},i}) dL, \tag{11}$$

C is the solute concentration [g/kg], ρ_{solv} is the density of the solvent [kg/m^3], ρ_i is the density of the i-form crystals [kg/m^3], k_{vi} is the volumetric shape factor of the i-form crystals (dimensionless) as defined by $v_i = k_{vi}L^3$, where v_i is the volume of the i-form crystal [m^3], and 10^3 is a constant [g/kg] to ensure unit consistency. The kinetic expressions are

$$B_\alpha = k_{b\alpha}(S_\alpha - 1)\mu_{\alpha,3} \quad (\alpha\text{-form crystal nucleation rate}), \tag{12}$$

$$G_\alpha = \begin{cases} k_{g\alpha}(S_\alpha - 1)^{g_\alpha} & \text{if } S_\alpha \geq 1 \\ k_{d\alpha}(S_\alpha - 1) & \text{otherwise} \end{cases} \quad (\alpha\text{-form crystal growth/dissolution rate}), \tag{13}$$

$$B_\beta = k_{b\beta,1}(S_\beta - 1)\mu_{\alpha,3} + k_{b\beta,2}(S_\beta - 1)\mu_{\beta,3} \quad (\beta\text{-form crystal nucleation rate}), \tag{14}$$

$$G_\beta = k_{g\beta,1}(S_\beta - 1)^{g_\beta} \exp\left(-\frac{k_{g\beta,2}}{S_\beta - 1}\right) \quad (\beta\text{-form crystal growth rate}), \tag{15}$$

where $S_i = C/C_{\text{sat},i}$ and $C_{\text{sat},i} = a_{i,1}T^2 + a_{i,2}T + a_{i,3}$ are the supersaturation and the saturation concentration [g/kg] of the i-form crystals, and T is the solution temperature [°C]. The kinetic parameters $k_{b\alpha}$, $k_{g\alpha}$, and $k_{d\alpha}$ correspond to the nucleation [#/m^{3}s], growth [m/s], and dissolution [m/s] rates of α-form crystals, whereas $k_{b\beta,j}$ and $k_{g\beta,j}$ correspond to the jth nucleation [#/m^{3}s] and growth [m/s] for $j = 1$ and

Table 1. Model Parameters for the Polymorphic Crystallization of L-Glutamic Acid (Model Parameter Values Were Obtained by Bayesian Estimation[49])

Parameters	Values	Parameters	Values
$\ln k_{b\alpha}$	17.233	ρ_{solv}	990
$\ln k_{g\alpha,0}$	1.878	ρ_α	1540
g_α	1.859	ρ_β	1540
$\ln E_{g\alpha}$	10.671	$k_{v\alpha}$	0.480
$\ln k_{d\alpha}$	−10.260	$k_{v\beta}$	0.031
$\ln k_{b\beta,1}$	15.801	$a_{\alpha,1}$	8.437×10^{-3}
$\ln k_{b\beta,2}$	20.000	$a_{\alpha,2}$	0.03032
$\ln k_{g\beta,0}$	52.002	$a_{\alpha,3}$	4.564
$\ln k_{g\beta,2}$	−0.251	$a_{\beta,1}$	7.644×10^{-3}
$g\beta$	1.047	$a_{\beta,2}$	−0.1165
$\ln E_{g\beta}$	12.078	$a_{\beta,3}$	6.622

dimensionless for $j = 2$ rates of β-form crystals, and g_i is the growth exponential constant of the i-form crystals which may have a value between 1 (for diffusion-limited growth) and 2 (for surface integrationlimited growth).[43] The Arrhenius equation was used to account for the variability of crystal growth rate with temperature:

$$k_{g\alpha} = k_{g\alpha,0} \exp\left(-\frac{E_{g\alpha}}{8.314(T+273)}\right), \quad (16)$$

$$k_{g\beta,1} = k_{g\beta,0} \exp\left(-\frac{E_{g\beta}}{8.314(T+273)}\right), \quad (17)$$

where $k_{gi,0}$ and E_{gi} are the pre-exponential factor [m/s] and activation energy [J/mol] for the growth rate of i-form crystals. The nominal values for the model parameters are given in Table 1. The partial differential Eqs. 8 and 9 are discretized into a series of ODEs as in Eq. 2. The resulting discretizations of $f_{seed,i}$ and $f_{nucl,i}$ with respect to L together with the solute concentration are considered as the system states.

Of all the system states, only solute concentration is measured. Hence, the rest of the system states need to be estimated from available measurements. In this study, the following measurements are considered:

$$y = [\mu_{\alpha,1}, \mu_{\alpha,2}, \mu_{\beta,1}, \mu_{\beta,2}, X_\alpha, C, T]^T, \quad (18)$$

where X_α is the crystal concentration of α-form crystals. The first four variables (i.e., the first- and second-order moments of α- and β-form crystals) can be measured using the online high-speed imaging system developed by the pharmaceutical manufacturer GlaxoSmithKline.[45] The crystal concentration of α-form crystals can be measured by Raman Spectroscopy.[41,42] Several online techniques are available for measuring the solution concentration such as conductivity or attenuated total reflection Fourier transform infrared spectro-

Table 2. The Parameters Describing the Seed Distributions

Seed	Mass Density [g/kg]	Mean Crystals size [μm]	Standard Deviation of Crystals Size [μm]
α	10.0	100.0	10.0
β	1.0	100.0	10.0

Table 3. Tuning Parameters for the NMPC Strategy

Values for Objective J_1	Values for Objective J_2
$W_{p,1} = I$	$W_{p,2} = I$
$(W_{u,1})_{i,i}* = 7[1 + 10(i-1)] \times 10^{-4}$	$(W_{u,2})_{i,i}* = [1+2(i-1)] \times 10^{-4}$
$W_\varepsilon = 10I$	$W_\varepsilon = 10I$
$w_\varepsilon = 10\,[1,1,\ldots,1]^T$	$w_\varepsilon = 10\,[1,1,\ldots,1]^T$
$W_0^\circ = 0.8$	$W_0^\circ = 0.8$
$\gamma = 0.1$	$\gamma = 0.1$

*The diagonal elements of matrices $W_{u,1}$ and $W_{u,2}$ where $i = 1,\ldots,N - k$.

scopy (ATR-FTIR).[5,46] Temperature measurements are readily available using teflon-coated thermocouples.

In this study, two objectives are considered for the polymorphic transformation of α- to β-form crystals. The first objective is to maximize the mass of β-form crystals, which is equivalent to maximizing the third-order moment or the yield of β-form crystals. In relation to the objective function in Eq. A6 this objective can be written as

$$J_1 = \min_\Phi [P_1 - P_{1,d}]^T W_{p,1}[P_1 - P_{1,d}] + \Phi^T W_{u,1}\Phi, \quad (19)$$

where $P_1 = (\mu_{\beta,3})_{t=t_f}$, $P_{1,d}$ can be set arbitrarily large as long as it is greater than the achievable value of $\mu_{\beta,3}$ ($P_{1,d} = 0.5$ is used in this study), t_f is the batch time, and $\Phi = [\Delta T_k, \Delta T_{k+1}, \cdots, \Delta T_{N-1}]^T$. The second objective is to minimize the ratio of the nucleated crystal mass to the seed crystal mass of β-form crystals, which can be written as

$$J_2 = \min_\Phi [P_2 - P_{2,d}]^T W_{p,2}[P_2 - P_{2,d}] + \Phi^T W_{u,2}\Phi, \quad (20)$$

where $P_2 = (\mu_{\beta,3}^{nucl}/\mu_{\beta,3}^{seed})_{t=t_f}$ and $P_{2,d} = 0$. These optimization objectives are subject to the model equations and the inequality constraints

$$T_{min} \leq T(t) \leq T_{max}, \quad (21)$$

$$C_{sat,\beta}(t) < C(t) < C_{sat,\alpha}(t), \quad (22)$$

$$C(t_f) \leq C_{max}(t_f), \quad (23)$$

where $T_{min} = 25°C$ and $T_{max} = 50°C$ are the minimum and maximum temperatures due to the limitation of water bath heating/cooling. The state constraints (22) aims to prevent the nucleation and growth of α- form crystals and the dissolution of β-form crystals during polymorphic transformation. The endpoint state constraint (23) ensures that the minimum yield required by economic considerations is satisfied. Practically, if

Table 4. Variations in Model Parameters for Robustness Study: Case 1 is the Norminal Model, Case 2 Has Slow Nucleation and Fast Growth Rate Parameters for β-Form Crstals, and Case 3 Has Fast Nucleation and Slow Growth Rate Parameters for β-Form Crystals

Cases	$\ln(k_{b\beta,1})$	$\ln(k_{b\beta,2})$	$\ln(k_{g\beta,0})$	$\ln(k_{g\beta,2})$	g_β	$\ln(E_{g\beta})$
1	15.801	20.000	52.002	−0.251	1.047	12.078
2	15.758	19.961	53.200	−0.280	1.100	12.060
3	15.842	20.036	50.883	−0.240	1.019	12.070
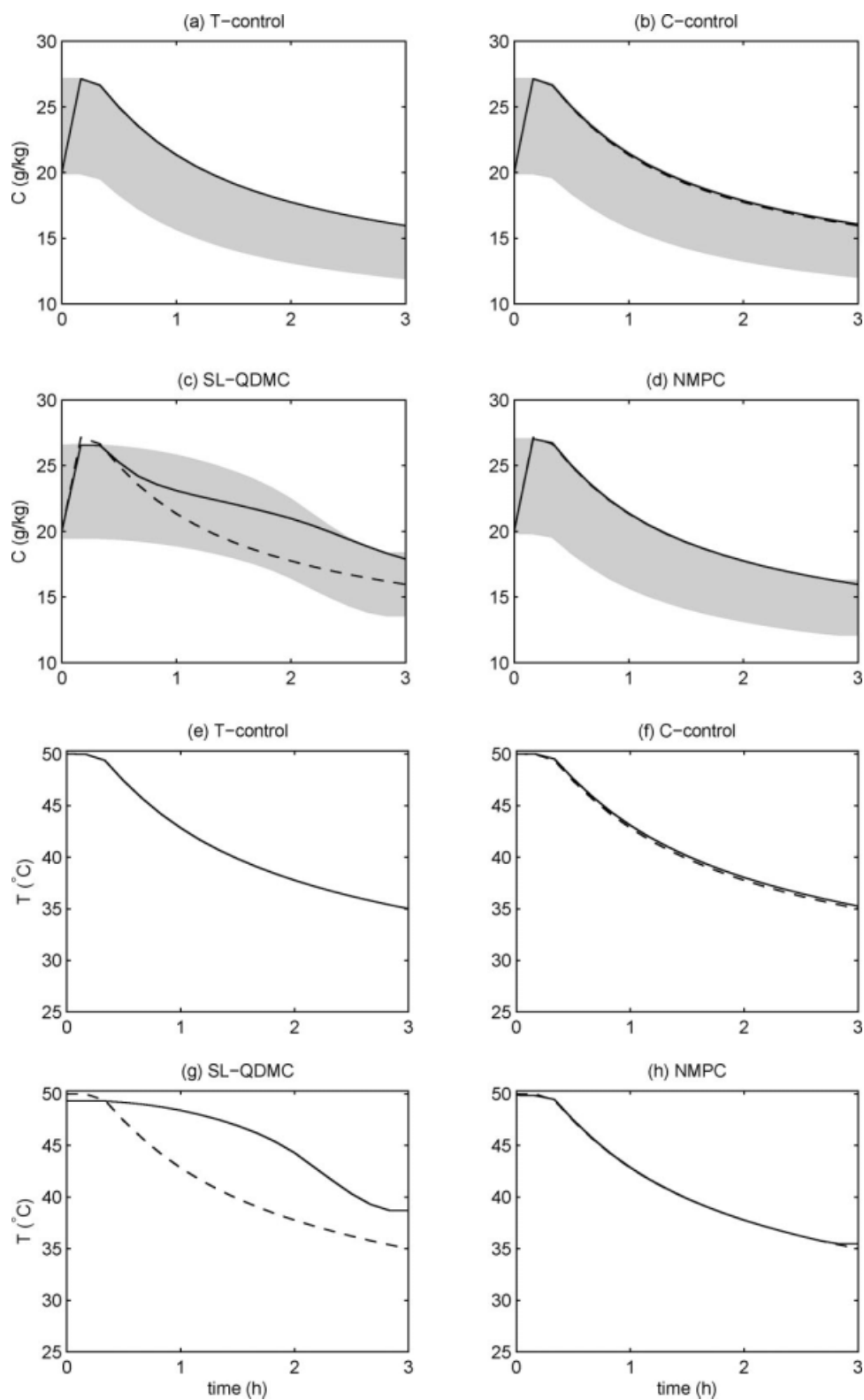
Figure 2. Concentration and temperature trajectories for case 1 with objective J_1.

The solid lines are trajectories corresponding to the four control strategies studied, the dashed lines are the optimal trajectories, and the shaded region indicates the inequality constraint (22) corresponding to the control strategies.
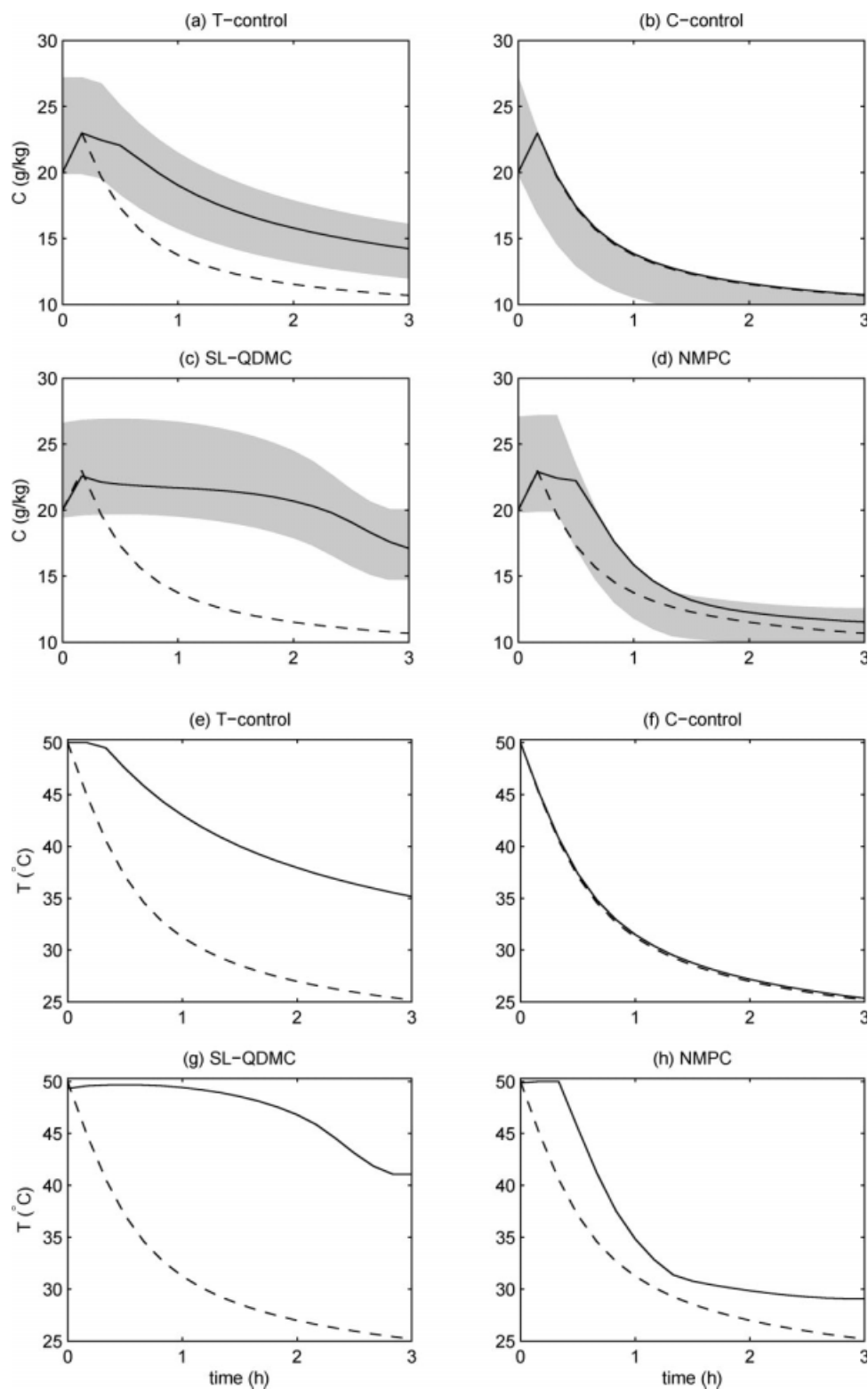
Figure 3. Concentration and temperature trajectories for case 2 with objective J_1.

The solid lines are trajectories corresponding to the four control strategies studied, the dashed lines are the optimal trajectories, and the shaded region indicates the inequality constraint (22) corresponding to the control strategies.

constraint (23) is not satisfied at $t = t_f$, then the batch time can be extended until it is satisfied with reduction in batch productivity.

Simulation Results and Discussion

In the polymorphic transformation, both α- and β-form crystals are seeded according to a Gaussian distribution with

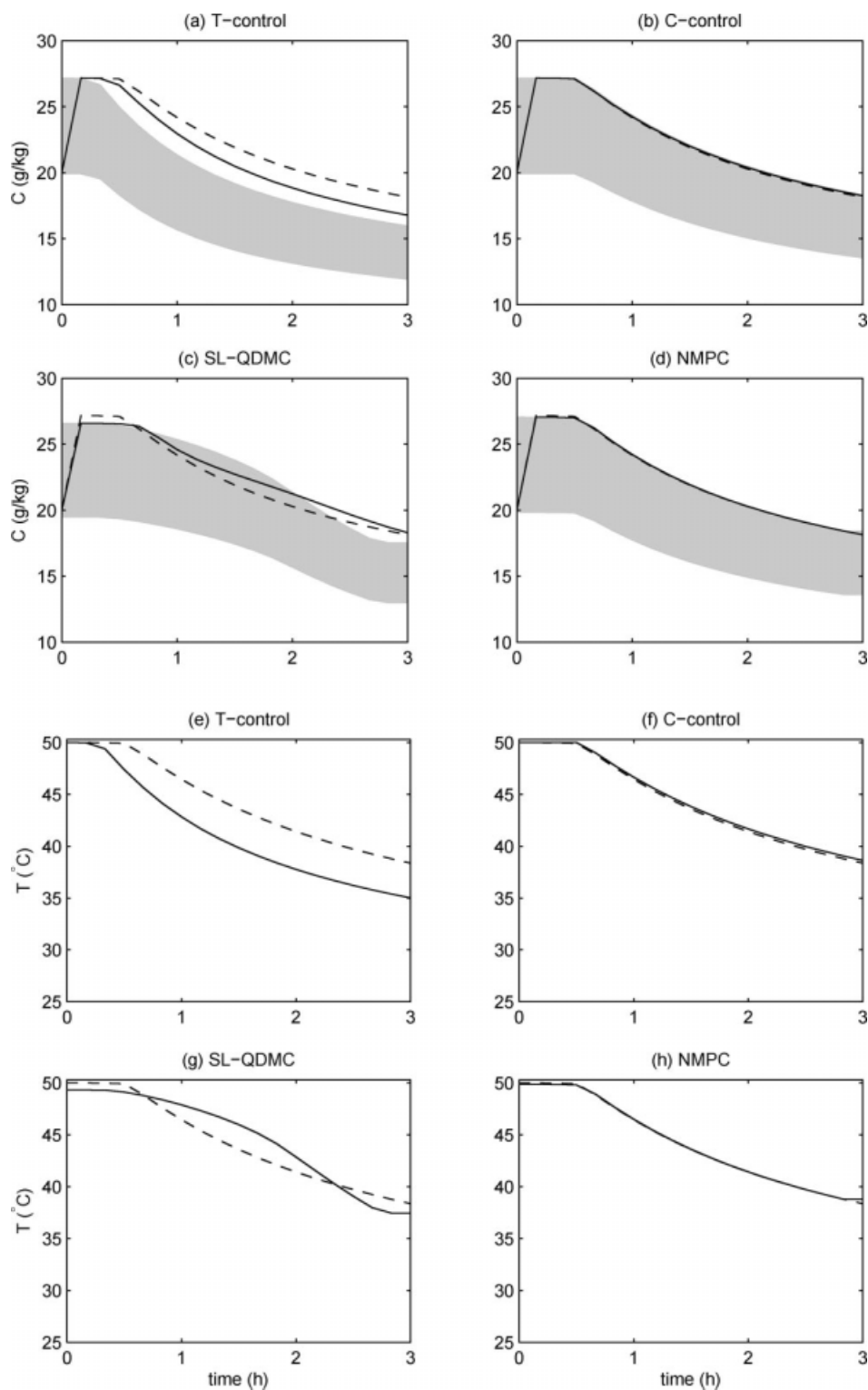**Figure 4. Concentration and temperature trajectories for case 3 with objective J_1.**

The solid lines are trajectories corresponding to the four control strategies studied, the dashed lines are the optimal trajectories, and the shaded region indicates the inequality constraint (22) corresponding to the control strategies.

parameter values given in Table 2. The initial solute concentration C_0 and maximum final solute concentration $C_{max}(t_f)$ are 20 g/kg with a default batch time t_f is 3 h which is extended if the inequality constraint (23) is not satisfied at that time.

Description of specific control implementations

The tuning parameters for the NMPC strategy for both objectives are given in Table 3. The performance and robustness of the NMPC strategy to the perturbations in the kinetic

Table 5. Values of the Control Objective P_1 for Various Control Strategies for the Three Sets of Model Parameters in Table 4

Cases	T-Control	C-Control	SL-QDMC	NMPC	Optimal
1	0.3119	0.3099	0.2720	0.3117	0.3119
2	0.3478	0.4187	0.2881	0.4031	0.4195
3	0.2569	0.2630	0.2634	0.2666	0.2667

parameters in Table 4 are compared with that of T-control, C-control, and quadratic dynamic matrix control with successive linearization (SL-QDMC). T-control is the most widely studied approach for the optimal control of crystallization processes in which the temperature trajectory is computed from the optimization of an objective function based on an offline model with nominal parameters. The comparison in this paper implements the standard formulation in which the temperature-time trajectory is parameterized as a first-order spline with 18 time intervals (10 min). In many experimental and simulation studies of batch crystallizations, C-control has resulted in low sensitivity of the product quality to most practical disturbances and variations in kinetic parameters.[9,13–16,40,47,48] This comparison implements the most popular C-control strategy in which the concentration-temperature trajectory obtained from nominal T-control is parameterized and the resulting parametrization is used to calculate the setpoint for the temperature feedback control loop throughout the batch.[40,47,48] The formulation of SL-QDMC is based on the quadratic dynamic matrix control (QDMC) by Garcia and Morshedi,[49] with the successive linearization of the process model performed to obtain the dynamic matrix at every sampling instance. The constraints are handled in a similar way as in the NMPC strategy.

Comparison results and discussion

For the first control objective J_1, the concentration and temperature trajectories for all four control strategies compared to the corresponding optimal trajectories, for the three sets of parameters, are shown in Figures 2–4.[†] The corresponding values of P_1 (which is proportional to the mass yield of β crystals) are in Table 5. The optimal control trajectory for this objective is very close to the solubility curve of α-form crystals (see Figure 2a) due to the slow growth rate of β-form crystals relative to the dissolution rate of α-form crystals. As a result, the optimal solution is to maximize the supersaturation with respect to the solubility of the β-form crystals while operating between the two solubility curves. When there is no plant-model mismatch (Figure 2), all control strategies except SL-QDMC produce similar results which are very close to the optimal solution.

The T-control strategy is not robust for the modelling error given by Case 2, with the temperature trajectory deviating significantly from the optimal trajectory and the resulting P_1 value is 17% lower than the optimal one (Figure 3 and Table 5). For Case 3 (Figure 4), the T-control strategy violates one of the constraints most of the time during the batch. In contrast, the C-control strategy provides very good robustness in

all cases, producing P_1 values within 1% of the optimal ones. The robustness of the C-control strategy for this objective is in agreement with an earlier report which used a different kinetic model.[40] The poor performance of the SL-QDMC for Cases 1 and 2 with P_1 values 13 and 31% lower than optimal may be accounted for by the high process nonlinearity and the closeness of the optimal solution to a constraint, the solubility curve of α-form crystals. This closeness to the constraint prevents the use of aggressive tuning parameters for SL-QDMC, otherwise the constraint is violated even for Case 1 with no model uncertainty. SL-QDMC results in good performance for Case 3 with a P_1 value within 2% of the optimal one, but violates a state constraint near the end of the batch (Figure 4c).

The NMPC strategy shows good robustness for Case 3, but it is less robust for Case 2. Although the temperature and concentration trajectories for the NMPC strategy for Case 2 are different from the optimal trajectories (Figure 3), the P_1 value is nearly optimal (i.e., within 4%) for all three sets of parameters.

Objective J_2 is more sophisticated than objective J_1. For objective J_1, the purpose is to maximize the yield of β. Physically, this can be done when the nucleation and growth rates of β-form crystals are maximized. On the other hand, objective J_2 is equivalent to maximizing the yield of β-form crystals while trying to simultaneously minimize its nucleation. This results in maintaining a tradeoff between the nucleation and growth rates of β-form crystals. For objective J_2, the temperature and concentration trajectories obtained by the four control strategies are plotted in Figures 5–7 with P_2 values tabulated in Table 6. The optimal solute concentration at the end of the batch is equal to the predefined $C_{max}(t_f)$ for all three sets of parameters. For solute concentration and temperature considered here, the nucleated mass of β-form crystals always increases at a faster rate than the seed mass of β-form crystals. As the β-form crystals nucleate and grow, the ratio of nucleated crystal mass to seed crystal mass of β-form crystals always increases. As a result, any value of $C_{max}(t_f)$ lower that the value specified by its upper bound constraint at 20 g/kg would increase the objective J_2 and would not be optimal.

For Case 1 (Figure 5), all control strategies except SL-QDMC produce nearly the optimal P_2 value (Table 6). The performance of T-control for Case 2 is poor (Figure 6), with a P_2 value 39% higher than optimum. Implementing T-control in Case 3 (Figure 7) needs an extension of the batch time to 4.5 h in order to satisfy the inequality constraint on the yield (23). The P_2 value obtained by C-control is much better than obtained by the T-control for Case 2 but only moderately better for Case 3 (Table 6). This improved robustness is achieved, however, by using a longer batch time, requiring about 50 h (Case 2) and 5.8 h (Case 3) to satisfy the inequality constraint (23). When there is no plant-model mismatch, SL-QDMC resulted in the poorest performance. For Cases 2 and 3, the P_2 values of SL-QDMC are worse than C-control and NMPC but the difference is not nearly as big as in Case 1. For all three sets of parameters, SL-QDMC was able to satisfy all the constraints for the second objective within the specified batch time.

For the second objective, the NMPC strategy had the best performance and robustness among the four control strategies for both sets of perturbed parameters, with P_2 values

---

[†]The optimal temperature trajectory was computed by applying T-control to the sets of parameters treated as known.
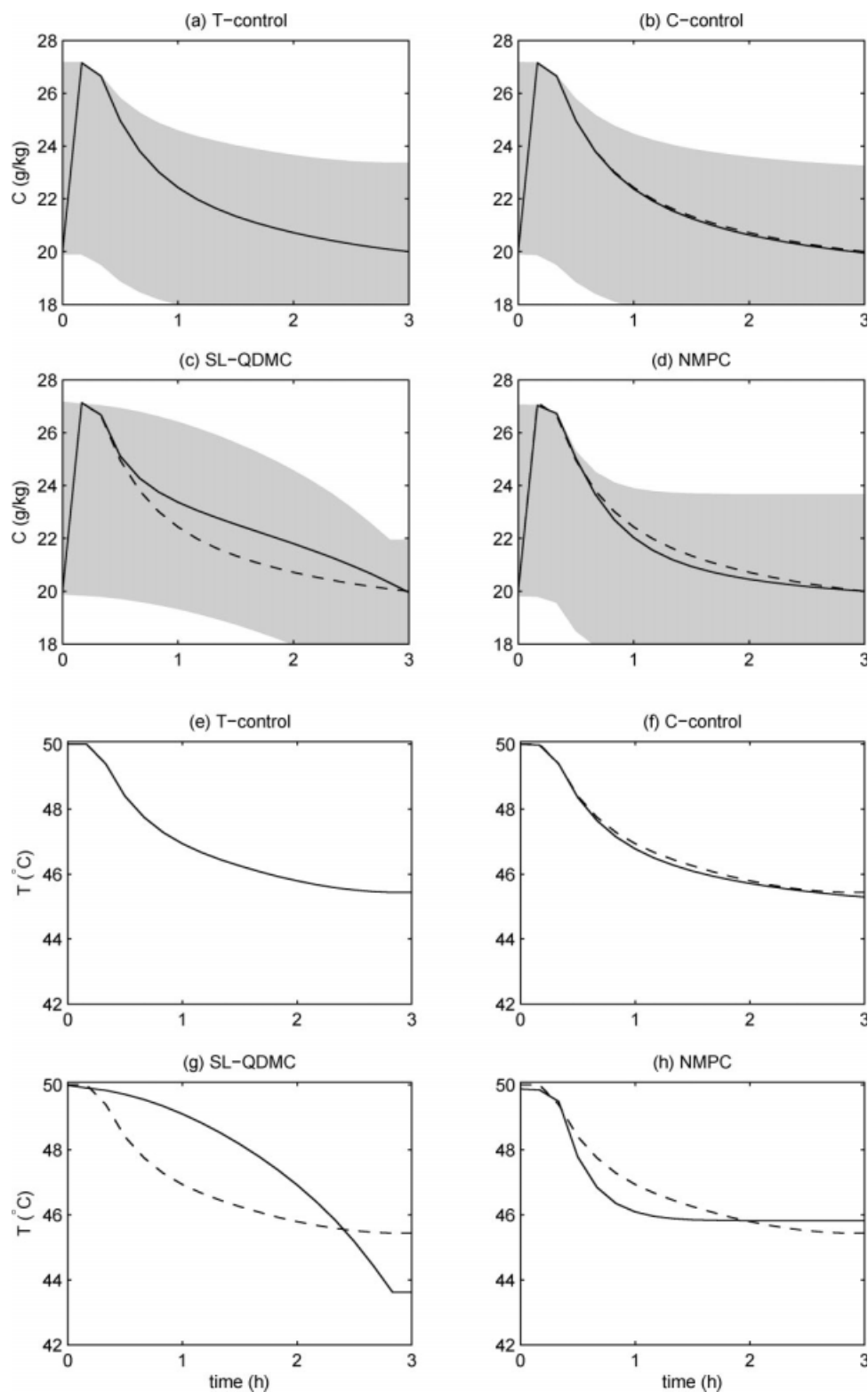
Figure 5. Concentration and temperature trajectories for case 1 with objective J_2.

The solid lines are trajectories corresponding to the four control strategies studied, the dashed lines are the optimal trajectories, and the shaded region indicates the inequality constraint (22) corresponding to the control strategies.

within 7% from the optimal ones. Although C-control and NMPC gave nearly the same P_2 values and both satisfied all of the constraints during the entire batch, a clear advantage of NMPC was that it completed the batches within the specified batch time. Although the greater ease of implementation of C-control makes it easier to transfer to industry,[16,48] this
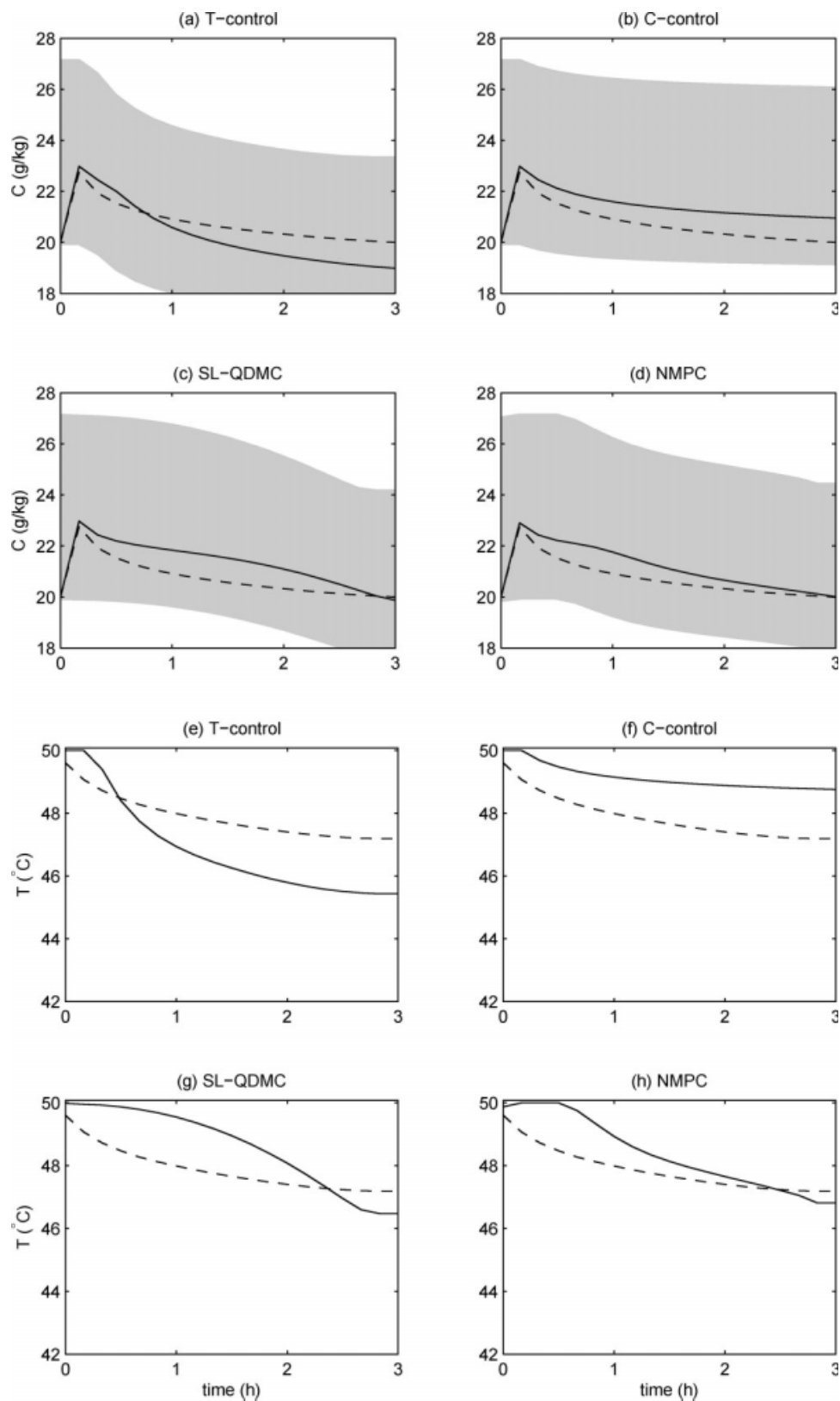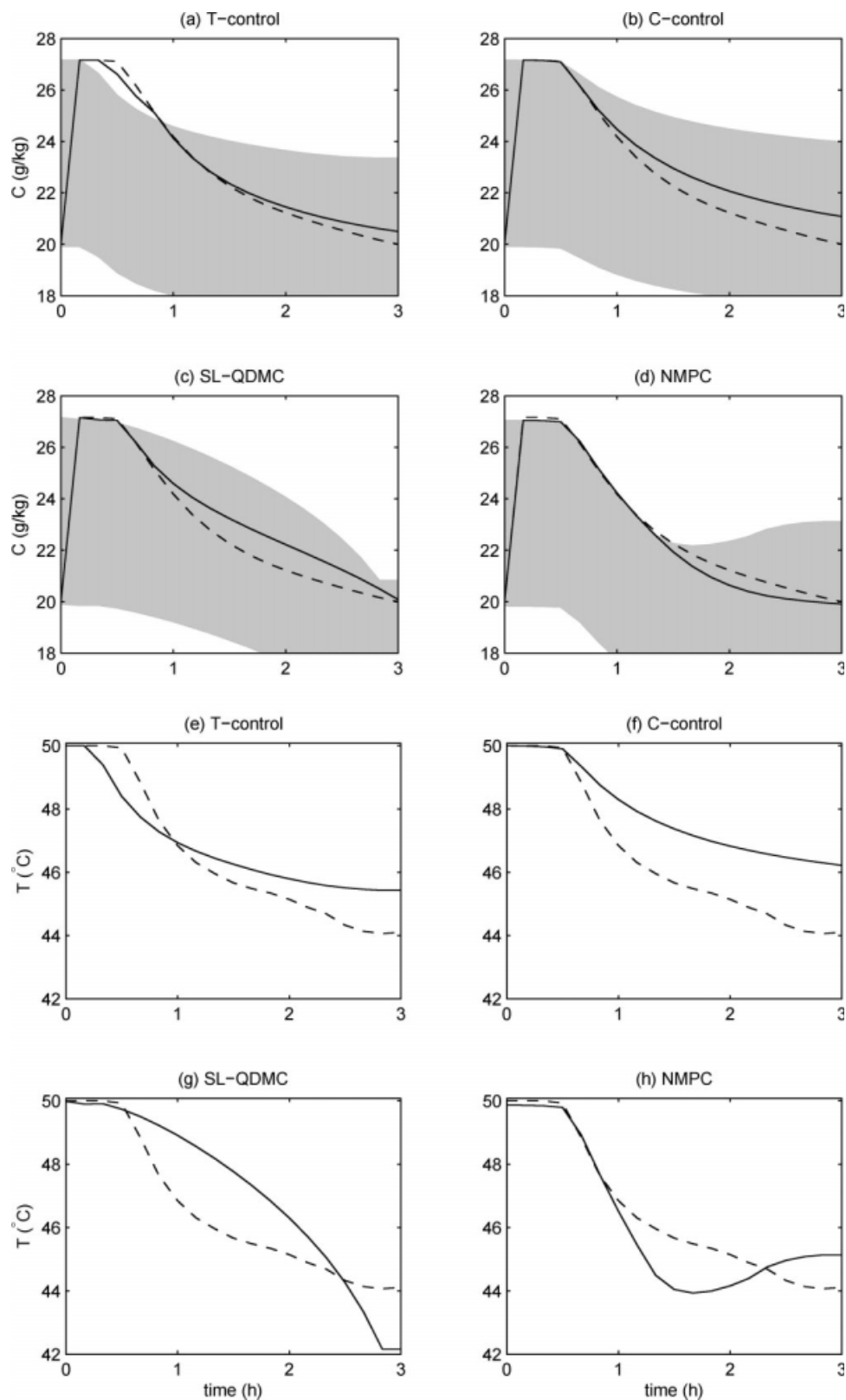
Figure 6. Concentration and temperature trajectories for case 2 with objective J_2.

The solid lines are trajectories corresponding to the four control strategies studied, the dashed lines are the optimal trajectories, and the shaded region indicates the inequality constraint (22) corresponding to the control strategies.

Figure 7. Concentration and temperature trajectories for case 3 with objective J_2.

The solid lines are trajectories corresponding to the four control strategies studied, the dashed lines are the optimal trajectories, and the shaded region indicates the inequality constraint (22) corresponding to the control strategies.

Table 6. Values of the Control Objective P_2 for Various Control Strategies for the Three Sets of Model Parameters in Table 4

Cases	T-Control	C-Control	SL-QDMC	NMPC	Optimal
1	0.0381	0.0385	0.0406	0.0384	0.0381
2	0.0064	0.0050*	0.0053	0.0049	0.0046
3	0.0683*	0.0679*	0.0681	0.0679	0.0659

*These values are obtained after the batch time was extended to satisfy constraint (23).

simulation study demonstrates that there is room for improved robust performance and productivity by using a more sophisticated NMPC strategy.

Conclusions

An NMPC strategy based on EPSAC and UKF was presented for batch polymorphic crystallization processes. A simulation study considered the control objectives of maximizing the yield of β-form crystals (P_1) and minimizing the ratio of nucleated crystal mass to seed crystal mass of β-form crystals (P_2). The performance and robustness of the NMPC strategy was compared to established control strategies, namely T-control, C-control, and SL-QDMC.

T-control was very sensitive to parameter perturbations, especially for Case 2, which results in 17 and 39% deviation from the optimal values of P_1 and P_2, respectively. C-control was robust for the maximization of yield, which produced almost identical results to the optimal values for three sets of parameters. Although C-control satisfied all of the constraints and produced P_2 values better or similar to those of the other control strategies, the simulation study showed that C-control could take a very long batch time to satisfy the yield constraint (23). SL-QDMC performed very poorly, even when there is no plant-model mismatch, due to high process nonlinearity exacerbated by closeness of the optimal solution to a state constraint. The NMPC strategy showed good overall robustness for both objectives (within 4 and 7% of the optimal values, respectively) while satisfying all constraints within the specified batch time.

Literature Cited

1. Brittain HG. The impact of polymorphism on drug development: a regulatory viewpoint. *Am Pharm Rev*. 2003;3:67–70.
2. Blagden N, Davey R. Polymorphs take shape. *Chem Brit*. 1999;35: 44–47.
3. Hu Q, Rohani S, Jutan A. Modelling and optimization of seeded batch crystallizers. *Comput Chem Eng*. 2005;29:911–918.
4. Larsen PA, Patience DB, Rawlings JB. Industrial crystallization process control. *IEEE Contr of Syst Mag*. 2006;26:70–80.
5. Rawlings JB, Miller SM, Witkowski WR. Model identification and control of solution crystallization processes: a review. *Ind Eng Chem Res*. 1993;32:1275–1296.
6. Worlitschek J, Mazzotti M. Model-based optimization of particle size distribution in batch-cooling crystallization of paracetamol. *Cryst Growth Des*. 2004;4:891–903.
7. Zhang GP, Rohani S. On-line optimal control of a seeded batch cooling crystallizer. *Chem Eng Sci*. 2003;58:1887–1896.
8. Braatz RD, Fujiwara M, Wubben T, Rusli E. Crystallization: particle size control. In: Swarbrick J, editor. *Encyclopedia of Pharmaceutical Technology*, 3rd ed. New York: Marcel Dekker, 2006 (invited).
9. Rohani S, Horne S, Murthy K. Control of product quality in batch crystallization of pharmaceuticals and fine chemicals. Part 2: external control. *Org Process Res Dev*. 2005;9:873–883.
10. Diehl M, Bock HG, Kostina E. An approximation technique for robust nonlinear optimization. *Math Program Ser B*. 2006;107:213–230.
11. Ma DL, Braatz RD. Worst-case analysis of finite-time control policies. *IEEE Trans Contr Syst Technol*. 2001;9:766–774.
12. Srinivasan B, Bonvin D, Visser E, Palanki S. Dynamic optimization of batch processes—II. Role of measurements in handling uncertainty. *Comput Chem Eng*. 2003;27:27–44.
13. Fujiwara M, Chow PS, Ma DL, Braatz RD. Paracetamol crystallization using laser backscattering and ATR-FTIR spectroscopy: metastability, agglomeration and control. *Cryst Growth Des*. 2002;2:363–370.
14. Fujiwara M, Nagy ZK, Chew JW, Braatz RD. First-principles and direct design approaches for the control of pharmaceutical crystallization. *J Process Control*. 2005;15:493–504.
15. Gron H, Borissova A, Roberts KJ. In-process ATR-FTIR spectroscopy for closed-loop supersaturation control of a batch crystallizer producing monosodium glutamate crystals of defined size. *Ind Eng Chem Res*. 2003;42:198–206.
16. Liotta V, Sabesan V. Monitoring and feedback control of supersaturation using ATR-FTIR to produce an active pharmaceutical ingredient of a desired crystal size. *Org Process Res Dev*. 2004;8: 488–494.
17. De Keyser RMC, Cauwenberghe ARV. Extended prediction self-adaptive control. In: *IFAC Symp. on Identification and System Parameter Estimate*, 1985:1255–1260.
18. Garcia CE, Prett DM, Morari M. Model predictive control: theory and practice - a survey. *Automatica*. 1989;25:1753–1758.
19. Qin SJ, Badgwell TA.An overview of industrial model predictive control technology. Kantor J, Garcia CE, Carnahan B, editors. *Chemical Process Control - AIChE Symposium Series*. New York: AIChE, 1997:232–256.
20. Henson MA. Nonlinear model predictive control: current status and future directions. *Comput Chem Eng*. 1998;23:187–202.
21. Morari M, Lee JH. Model predictive control: past, present and future. *Comput Chem Eng*. 1999;23:667–682.
22. Camacho EF, Bordons C. *Model Predictive Control*. London: Springer-Verlog, 1999.
23. Rawlings JB. Tutorial overview of model predictive control. *IEEE Control Syst Mag*. 2000;20:38–52.
24. De Prada C, Sarabia D, Cristea S, Mazaeda R. Plant-wide control of a hybrid process. *Int J Adapt Control*. 2008;22:124–141.
25. Eaton JW, Rawlings JB. Feedback-control of chemical processes using online optimization techniques. *Comput Chem Eng*. 1990;14: 469–479.
26. Kalbasenka AN, Spierings LCP, Huesman AEM, Kramer HJM. Application of seeding as a process actuator in a model predictive control framework for fed-batch crystallization of ammonium sulphate. *Part Part Syst Charact*. 2007;24:40–48.
27. Nagy ZK, Braatz RD. Robust nonlinear model predictive control of batch processes. *AIChE J*. 2003;49:1776–1786.
28. Rohani S, Haeri M, Wood HC. Modeling and control of a continuous crystallization process - part 2. Model predictive control. *Comput Chem Eng*. 1999;23:279–286.
29. Tadayyon A, Rohani S. Extended Kalman filter-based nonlinear model predictive control of a continuous KCl-NaCl crystallizer. *Can J Chem Eng*. 2001;79:255–262.
30. De Keyser R, Donald J III. Application of the NEPSAC nonlinear predictive control strategy to a semiconductor reactor. *Lecture Notes Control Inform Sci*. 2007;358:407–417.
31. Ionescu C, De Keyser RMC. EPSAC predictive control of blood glucose level in type I diabetic patients. In: *Proceedings of the 44th Conference on Decision and Control, and the European Control Conference*. 2005;4845–4850.
32. Rueda A, Cristea S, Prada CD, De Keyser RMC. Non-linear predictive control for a distillation column. In: *Proceedings of the 44th IEEE Conference on Decision and Control, and the European Control Conference*. 2005;5156–5161.
33. Tamas L, Nascu I, De Keyser R. The NEPSAC nonlinear predictive controller in a real life experiment. In: *International Conference on Intelligent Engineering Systems*. 2007:229–234.
34. Julier SJ. The scaled unscented transformation. In: *Proceedings of the American Control Conference*, Vol. 6, 2002:4555–4559.

35. Julier SJ. The spherical simplex unscented transformation. In: *Proceedings of the American Control Conference*, Vol. 3, 2003:2430–2434.
36. Julier SJ, Uhlmann JK. Reduced sigma point filters for the propagation of means and covariances through nonlinear transformation. In: *Proceedings of the American Control Conference*, Vol. 2, 2002:887–892.
37. Julier SJ, Uhlmann JK. Unscented filtering and nonlinear estimation. *Proc IEEE*. 2004;92:401–422.
38. Julier SJ, Uhlrnann JK, Durrant-Whyte HF. A new approach for filtering nonlinear systems. In: *Proceedings of the American Control Conference*, 1995:1628–1632.
39. Scokaert POM, Rawlings JB. Feasibility issues in linear model predictive control. *AIChE J*. 1999;45:1649–1659.
40. Hermanto MW, Chiu MS, Woo XY, Braatz RD. Robust optimal control of polymorphic transformation in batch crystallization. *AIChE J*. 2007;53:2643–2650.
41. Ono T, Kramer HJM, Ter Horst JH, Jansens PJ. Process modeling of the polymorphic transformation of L-glutamic acid. *Cryst Growth Des*. 2004;4:1161–1167.
42. Scholl J, Bonalumi D, Vicum L, Mazzotti M. In situ monitoring and modeling of the solvent-mediated polymorphic transformation of L-Glutamic acid. *Cryst Growth Des*. 2006;6:881–891.
43. Mersmann A. *Crystallization Technology Handbook* 2nd ed. Florida, USA: CRC Press, 2001.
44. Hermanto MW, Kee NC, Tan RBH, Chiu MS, Braatz RD. Robust Bayesian estimation of kinetics for the polymorphic transformation of L-glutamic acid crystals. *AIChE J*. 2008;54:3248–3259.
45. De Anda JC, Wang XZ, Roberts KJ. Multi-scale segmentation image analysis for the in-process mon-itoring of particle shape with batch crystallisers. *Chem Eng Sci*. 2005;60:1053–1065.
46. Togkalidou T, Tung HH, Sun Y, Andrews A, Braatz RD. Solution concentration prediction for pharma-ceutical crystallization processes using robust chemometrics and ATR FTIR spectroscopy. *Org Process Res Dev*. 2002;6:317–322.
47. Nagy ZK, Chew JW, Fujiwara M, Braatz RD. Comparative performance of concentration and temper-ature controlled batch crystallizations. *J Process Control*. 2008;18:399–407.
48. Zhou GX, Fujiwara M, Woo XY, Rusli E, Tung HH, Starbuck C, Davidson O, Ge Z, Braatz RD. Direct design of pharmaceutical antisolvent crystallization through concentration control. *Cryst Growth Des*. 2006;6:892–898.
49. Garcia CE, Morshedi AM. Quadratic programming solution of dynamic matrix control (QDMC). *Chem Eng Comm*. 1986;46:73–87.

Appendix

Formulation and Implementation of EPSAC-UKF NMPC Algorithm

EPSAC algorithm

The impulse response model for $z_{l,k+i}$ is

$$z_{l,k+i} = h_i \delta u_k + h_{i-1}\delta u_{k+1} + h_{i-2}\delta u_{k+2} + \cdots + h_{i-N_u+2}\delta u_{k+N_u-2}$$
$$+ h_{i-N_u+1}\delta u_{k+N_u-1} + \cdots + h_1 \delta u_{k+i-1}, \tag{A1}$$

where h_j is the jth impulse response coefficient. With $\delta u_{k+N_u-1} = \delta u_{k+N_u} = \cdots = \delta u_{k+i-1}$, this equation can be written as

$$z_{l,k+i} = h_i \delta u_k + h_{i-1}\delta u_{k+1} + h_{i-2}\delta u_{k+2} + \cdots$$
$$+ h_{i-N_u+2}\delta u_{k+N_u-2} + (h_1 + h_2 + \cdots + h_{i-N_u+1})\delta u_{k+N_u-1}$$
$$= h_i \delta u_k + h_{i-1}\delta u_{k+1} + h_{i-2}\delta u_{k+2} + \cdots$$
$$+ h_{i-N_u+2}\delta u_{k+N_u-2} + g_{i-N_u+1}\delta u_{k+N_u-1}, \tag{A2}$$

where g_j is the jth step response coefficient.

For convenience, $z_{l,k+i}$ can be represented as a linear function of g_j and $\Delta u_{l,j}$:

$$z_{l,k+i} = h_i \Delta u_{l,k} + h_{i-1}\sum_{j=0}^{1}\Delta u_{l,k+j} + h_{i-2}\sum_{j=0}^{2}\Delta u_{l,k+j} + \cdots$$
$$+ h_{i-N_u+2}\sum_{j=0}^{N_u-2}\Delta u_{l,k+j} + g_{i-Nu+1}\sum_{j=0}^{N_u-1}\Delta u_{l,k+j}$$
$$= (h_i + h_{i-1} + h_{i-2} + \cdots + h_{i-N_u+2} + g_{i-N_u+1})\Delta u_{l,k}$$
$$+ (h_{i-1} + h_{i-2} + \cdots + h_{i-N_u+2} + g_{i-N_u+1})\Delta u_{l,k+1} + \cdots$$
$$+ (h_{i-N_u+2} + g_{i-N_u+1})\Delta u_{l,k+N_u-2} + g_{i-N_u+1}\Delta u_{l,k+N_u-1}$$
$$= g_i\Delta u_{l,k} + g_{i-1}\Delta u_{l,k+1} + \cdots + g_{i-N_u+1}\Delta u_{l,k+N_u-1} \tag{A3}$$

Considering a batch process with the control horizon identical to the prediction horizon which covers from the next sampling time to the end of batch time denoted by $N_p = N_u = N - k$, where N is the total samples in a batch, the sequence of $z_{l,k+i}$ is

$$z_{l,k+1} = g_1\Delta u_{l,k},$$
$$z_{l,k+2} = g_2\Delta u_{l,k} + g_1\Delta u_{l,k+1},$$
$$\vdots$$
$$z_{l,N} = g_{N-k}\Delta u_{l,k} + g_{N-k-1}\Delta u_{l,k+1} + \cdots + g_1\Delta u_{l,N-1},$$

or

$$\mathbf{Z}_l = \mathbf{G}_l\Delta\mathbf{U}_l, \tag{A4}$$

where $\mathbf{Z}_l = [z_{l,k+1}, z_{l,k+2},\ldots,z_{l,N}]^T$, $\Delta\mathbf{U}_l = [\Delta u_{l,k}, \Delta u_{l,k+1},\ldots, \Delta u_{l,N-1}]^T$, and

$$\mathbf{G}_l = \begin{bmatrix} g_1 & 0 & \cdots & 0 \\ g_2 & g_1 & \cdots & 0 \\ \vdots & \vdots & \ddots & \vdots \\ g_{N-k} & g_{N-k-1} & \cdots & g_1 \end{bmatrix}$$

In summary, the future process variables of interest in the prediction horizon can be conveniently represented in matrix form as

$$\mathbf{Z} = \mathbf{Z}_b + \mathbf{G}_l\Delta\mathbf{U}_l, \tag{A5}$$

where $\mathbf{Z} = [z_{k+1}, z_{k+2},\ldots,z_N]^T$ and $\mathbf{Z}_b = [z_{b,k+1}, z_{b,k+2},\ldots,z_{b,N}]^T$.

Now consider an objective function J with single input ($n_u = 1$):

$$J = \min_{\Delta\mathbf{U}} \quad [\mathbf{P} - \mathbf{P}_d]^T\mathbf{W}_p[\mathbf{P} - \mathbf{P}_d] + \Delta\mathbf{U}^T\mathbf{W}_u\Delta\mathbf{U}, \tag{A6}$$

where $\mathbf{P}$, $\mathbf{P}_d$, and $\Delta\mathbf{U}$ are the vectors of the product quality, desired product quality, and the change in input variables, respectively, given by

$$\mathbf{P} = [p_{k+1}, p_{k+2}, \cdots, p_N]^T,$$
$$\mathbf{P}_d = [p_{d,k+1}, p_{d,k+2}, \cdots, p_{d,N}]^T,$$
$$\Delta\mathbf{U} = [\Delta u_k, \Delta u_{k+1}, \cdots, \Delta u_{N-1}]^T,$$

and $\mathbf{W}_p$ and $\mathbf{W}_u$ are the weight matrices for the product quality and the change in input variables, respectively. Then $\mathbf{P}$ and $\Delta\mathbf{U}$ can be decomposed into

$$P = P_b + G_{pl}\Delta U_l, \tag{A7}$$

$$\Delta U = \Delta U_b + \Delta U_l, \tag{A8}$$

where G_{pl} is the step response coefficient matrix corresponding to the product quality variable, and P_b is the predicted product quality calculated using the nonlinear model with predetermined future inputs $U_b = [u_{b,k},\ u_{b,k+1},\cdots,u_{b,N-1}]^T$, and

$$\Delta U_b = [\Delta u_{b,k}, \Delta u_{b,k+1}, \cdots, \Delta u_{b,N-1}]^T.$$

$$\Delta U_l = [\Delta u_{l,k}, \Delta u_{l,k+1}, \cdots, \Delta u_{l,N-1}]^T.$$

Hence, the minimization problem becomes:

$$
\begin{aligned}
J &= \min_{\Delta U_l} [(P_b - P_d) + G_{pl}\Delta U_l]^T W_p [(P_b - P_d) + G_{pl}\Delta U_l] \\
&\quad + [\Delta U_b + \Delta U_l]^T W_u [\Delta U_b + \Delta U_l] \\
&= \min_{\Delta U_l} \Delta U_l^T G_{pl}^T W_p G_{pl}\Delta U_l + 2(P_b - P_d)^T W_p G_{pl}\Delta U_l \\
&\quad + \Delta U_l^T W_u \Delta U_l + 2\Delta U_b^T W_u \Delta U_l \\
&= \min_{\Delta U_l} \Delta U_l^T \Gamma \Delta U_l + \psi^T \Delta U_l,
\end{aligned}
\tag{A9}
$$

where

$$\Gamma = G_{pl}^T W_p G_{pl} + W_u,$$

$$\psi = 2[(P_b - P_d)^T W_p G_{pl} + \Delta U_b^T W_u]^T.$$

The minimization is subject to the constraints $h(x_j, u_j) \leq 0$, $\forall j \geq k$, where k is the current sampling instance. For notational convenience, $h(x_j, u_j)$ is denoted as h_j, which can be decomposed into the base and linear part $h_j = h_{b,j} + h_{l,j}$. Therefore, the matrix form of the constraints in the prediction horizon is

$$H_b + G_{hl}\Delta U_l \leq 0, \tag{A10}$$

where G_{hl} is the step response coefficient matrix corresponding to the constraints function h_j and $H_b = [h_{b,k}, h_{b,k+1},\cdots,h_{b,N}]^T$.

From the authors' experience, when the constraints are highly nonlinear, handling (A10) directly will sometimes cause difficulty for the quadratic programming (QP) used for the optimization to find a feasible solution. Convergence was provided by the soft-constraint approach,[39] which replaces the minimization problem with

$$\min_{\Delta U_{l,\varepsilon}} J_{sc} \tag{A11}$$

subject to

$$H_b + G_{hl}\Delta U_l \leq \varepsilon, \tag{A12}$$

$$\varepsilon \geq 0, \tag{A13}$$

where $J_{sc} = J + \varepsilon^T W_\varepsilon \varepsilon + \varepsilon^T w_\varepsilon$, ε is a vector of slack variables, W_ε is a diagonal matrix of positive weight, and w_ε is a vector of positive elements. This modified minimization problem can be written as

$$
\begin{aligned}
J_{sc}^* &= \min_{\Delta U_{l,\varepsilon}} \Delta U_l^T \Gamma \Delta U_l + \psi^T \Delta U_l + \varepsilon^T W_\varepsilon \varepsilon + \varepsilon^T W_\varepsilon \\
&= \min_{\Delta U_{l,\varepsilon}} \begin{bmatrix} \Delta U_l^T & \varepsilon^T \end{bmatrix} \begin{bmatrix} \Gamma & 0 \\ 0 & W_\varepsilon \end{bmatrix} \begin{bmatrix} \Delta U_l \\ \varepsilon \end{bmatrix} + \begin{bmatrix} \psi^T & W_\varepsilon^T \end{bmatrix} \begin{bmatrix} \Delta U_l \\ \varepsilon \end{bmatrix} \\
&= \min_{\Pi} \Pi^T \Lambda \Pi + \tau^T \Pi,
\end{aligned}
$$
$$\tag{A14}$$

subject to

$$\begin{bmatrix} H_b \\ 0 \end{bmatrix} + \begin{bmatrix} G_{hl} & -I \\ 0 & -I \end{bmatrix} \Pi \leq 0. \tag{A15}$$

where $\Pi = [\Delta U_l^T, \varepsilon^T]^T$, $\Lambda = \begin{bmatrix} \Gamma & 0 \\ 0 & W_\varepsilon \end{bmatrix}$, and $\tau = [\psi^T, W_\varepsilon^T]^T$.

To summarize, the procedure for implementing the NMPC strategy based on EPSAC for each sampling instance k is:

(1) Obtain U_b by the following method:
- if $k = 0$ and *iter* $= 1$, U_b is chosen from the nominal operating point which was used in the previous batches;
- if $k > 0$ and *iter* $= 1$, U_b is set as the $U_{optimal}$ obtained in the previous sampling instance;
- if *iter* > 1, the updated U_b from the previous iteration is used;

where *iter* is the iteration count.

(2) Given the estimated current system states, obtain P_b and H_b by using U_b as the input to the nonlinear process model (1) to (5).

(3) Obtain the step response coefficient matrices G_{pl} and G_{hl} by introducing a step change in δu.

(4) Obtain $\Pi^* = [\Delta U_l^*, \varepsilon^*]^T$ from the solution to the minimization problem (A14) and (A15), then update the elements of U_b using

$$u_{b,k+j} = u_{b,k+j} + \sum_{i=0}^{j} \Delta u_{l,k+i},$$

where $j = 0, \ldots, N - 1 + k$.

(5) Calculate $err = \left\| \begin{bmatrix} G_{pl} \\ G_{hl} \end{bmatrix} \Delta U_l^* \right\|$. If *err* is greater than a specified tolerance[‡], *iter* $=$ *iter* $+ 1$, and go back to Step 1. Otherwise, set $U_{optimal} = U_b$ and implement the first element of $U_{optimal}$ to the process.

Unscented Kalman filter

Consider the $n\ (= n_x + n_y)$ dimensional augmented system states $x_{a,k} = [x_k, d_k]^T$ and recast the system Eq. 2 to 4 as

$$x_{a,k} = f_a(x_{a,k-1}, u_{k-1}) + w_{a,k-1}, \tag{A16}$$

$$y_k = g_a(x_{a,k}, u_k) + v_k, \tag{A17}$$

where

$$f_a(x_{a,k-1}, u_{k-1}) = \begin{bmatrix} f^T(x_{k-1}, u_{k-1}) & d_{k-1}^T \end{bmatrix}^T,$$

$$g_a(x_{a,k}, u_k) = g(x_k, u_k) + d_k,$$

$$w_{a,k-1} = \begin{bmatrix} w_k^T & \xi_k^T \end{bmatrix}^T.$$

[‡]1×10^{-4} was used in this study.

A summary of the UKF procedure is below:
(1) Calculate sigma points $\chi_{i,k-1}$ for $i = 0,1,\ldots,n+1$ by the spherical simplex unscented transformation as follows:
  (a) Obtain the initial weight sequence by specifying the weight for the first sigma point $\chi_{0,k-1}$, W_0°, which is a scalar weight for the mean value of the augmented system states. The initial weights for the rest of the sigma points are obtained as

$$W_i^0 = \frac{1 - W_0^{\circ}}{n+1} \quad \text{for } i = 1, \ldots, n+1. \tag{A18}$$

  (b) For $j = 2,3,\ldots,n$, generate the vector sequence by using the following equation:

$$X_i^j = \begin{cases} \begin{bmatrix} X_0^{j-1} \\ 0 \end{bmatrix} & \text{for } i = 0, \\ \begin{bmatrix} X_i^{j-1} \\ -\frac{1}{\sqrt{j(j+1)W_1^{\circ}}} \end{bmatrix} & \text{for } i = 1, \ldots, j, \\ \begin{bmatrix} 0_{j-1} \\ \frac{1}{\sqrt{j(j+1)W_1^{\circ}}} \end{bmatrix} & \text{for } i = j+1, \end{cases} \tag{A19}$$

where

$$X_0^1 = 0; \quad X_1^1 = -\frac{1}{\sqrt{2W_1^{\circ}}}; \quad X_2^1 = -\frac{1}{\sqrt{2W_1^{\circ}}}. \tag{A20}$$

  (c) Compute the unscaled sigma points according to:

$$X_{i,k-1}^{\circ} = \hat{x}_{a,k-1} + A^T X_i^n, \tag{A21}$$

where $\hat{x}_{a,k-1}$ and A^T are the mean of the augmented states and the Cholesky decomposition of the augmented states covariance matrix $P_{x_{a,k-1}}$ at previous sampling time, respectively. If $k = 1$, $\hat{x}_{a,0} = E[x_{a,0}]$ and $P_{x_{a,0}} = E[(x_{a,0} - \hat{x}_{a,0})(x_{a,0} - \hat{x}_{a,0})^T] = A^T A$. Otherwise, $\hat{x}_{a,k-1}$ and $P_{x_{a,k-1}}$ are defined in Step 7.
  (d) Calculate the scaled sigma points and their associated weights by

$$\chi_{i,k-1} = \chi_{0,k-1}^{\circ} + \gamma(\chi_{i,k-1}^{\circ} - \chi_{0,k-1}^{\circ}), \tag{A22}$$

$$W_i = \begin{cases} \frac{(w_0^{\circ} + \gamma^2 - 1)}{\gamma} & \text{for } i = 0, \\ \frac{W_i^{\circ}}{\gamma^2} & \text{for } i \neq 0, \end{cases} \tag{A23}$$

where $0 < \gamma \leq 1$ is a scaling factor indicating the distance of the sigma points to their mean values.

(2) Propagate the sigma points through the augmented system state equations:

$$\chi_{i,k|k-1} = f_a(\chi_{i,k-1}, u_{k-1}), \quad \text{for } i = 0, 1, \ldots, n+1. \tag{A24}$$

(3) Compute the predicted mean and covariance matrix of the augmented system states from

$$\hat{x}_{a,k|k-1} = \sum_{i=0}^{n+1} W_i \chi_{i,k|k-1}, \tag{A25}$$

$$P_{x_{a,k|k-1}} = \sum_{i=0}^{n+1} \left[W_i(\chi_{i,k|k-1} - \hat{x}_{a,k|k-1})(\chi_{i,k|k-1} - \hat{x}_{a,k|k-1})^T \right] + (1 - \gamma^2)(\chi_{0,k|k-1} - \hat{x}_{a,k|k-1})(\chi_{0,k|k-1} - \hat{x}_{a,k|k-1})^T + Q \tag{A26}$$

where Q is the process noise covariance matrix.
(4) Propagate $\chi_{i,k|k-1}$ through the observation equation:

$$y_{i,k|k-1} = g_a(\chi_{i,k|k-1}, u_k). \tag{A27}$$

(5) Compute the predicted mean and the covariance matrix of the measured variables:

$$\hat{y}_{k|k-1} = \sum_{i=0}^{n+1} W_i y_{i,k|k-1}, \tag{A28}$$

$$P_{y_{k|k-1}} = \sum_{i=0}^{n+1} \left[W_i(y_{i,k|k-1} - \hat{y}_{k|k-1})(y_{i,k|k-1} - \hat{y}_{k|k-1})^T \right] + (1 - \gamma^2)(y_{0,k|k-1} - \hat{y}_{k|k-1})(y_{0,k|k-1} - \hat{y}_{k|k-1})^T + R \tag{A29}$$

where R is the measurement noise covariance matrix.
(6) Compute the predicted cross-covariance matrix between the augmented system states and the measured variables from

$$P_{x_a y} = \sum_{i=0}^{n+1} W_i(\chi_{i,k|k-1} - \hat{x}_{a,k|k-1})(y_{i,k|k-1} - \hat{y}_{a,k|k-1})^T. \tag{A30}$$

(7) Once the measurement y_k is available, correct the predictions according to Kalman filter equations:

$$\hat{x}_{a,k} = \hat{x}_{a,k|k-1} + K_k(y_k - \hat{y}_{k|k-1}), \tag{A31}$$

$$P_{x_{a,k}} = P_{x_{a,k|k-1}} - K_k P_{y_{k|k-1}} K_k^T, \tag{A32}$$

where the Kalman gain K_k is defined as $K_k = P_{x_a y} P_{y_{k|k-1}}^{-1}$